

Effect of Heat Treatment on the Structural Characteristics and Dehydroxylation Kinetics of the Tunellite

MUGE SARI YILMAZ AND SABRIYE PISKIN*

*Yildiz Technical University Department of Chemical Engineering, Topkapı, Istanbul, Turkey.
piskin@yildiz.edu.tr**

(Received on 6th October 2011, accepted in revised form 26th January 2012)

Summary: The effect of heat treatment on the structural properties of the tunellite has been investigated in the present study. The tunellite samples were calcined in a furnace for 5 h at three different temperatures, 400, 710, and 800°C. These temperatures were determined with respect to the DTA/TG curve. The calcined tunellite samples were characterized by X-Ray Diffraction (XRD). It was found that with increasing calcination temperatures, a veatchite phase was observed. The morphology of the calcined tunellite samples was characterized by Scanning Electron Microscope (SEM). According to the results of the analyses, it was observed that the calcination temperature influenced the shape of the tunellite. The Brauner-Emmett-Teller (BET) analysis revealed that the specific surface area of the samples decreased with an increasing calcination temperature due to the shrinkage of the agglomerates. In addition, the dehydroxylation kinetics of the tunellite was studied by the thermogravimetric technique. The non-isothermal kinetic data were analyzed and the kinetic parameters for the dehydroxylation stage were computed by 21 solid-state mechanisms. In addition, the kinetic compensation effect (KCE) was also used in order to correlate the pre-exponential factor with the activation energy.

Introduction

Approximately 67% of the world's known boron reserves are found in Turkey. These high quality boron reserves are generally located in the regions of Bigadiç, Balıkesir, Kırka, and Kestelek in Turkey [1]. Unlike the other known boron reserves in Turkey, the Kırka borate deposits mainly consist of Na-, Na-Ca-, Ca-, Mg-, Mg-Ca-, and Sr-borate minerals [2]. Of these minerals, tunellite is a Sr-borate hydrate mineral that has been found in the Eskişehir, Kırka Boron deposits. The above mentioned mineral is a member of the borate series $M^{2+}O_3 \cdot 3B_2O_3 \cdot xH_2O$, with $M^{2+} = Sr$ and $x = 4$ and contains $n[B_6O_9(OH)_2]^{2-}$ polyanions [3].

The boron minerals and its compounds have a wide range of industrial applications. These minerals and compounds are widely used in nuclear technology, as abrasives and refractors in the glass and ceramic industry, in agriculture, as catalysts in the production of heat heat-resistant polymers, etc [4].

The structural changes in the boron minerals under the heat treatment have been investigated for many years [5-10]. When the boron minerals are heated, the mineral first loses the crystalline water at a temperature lower than 250°C and the structure water at a temperature higher than 250°C, and then recrystallizes into new phases. Subsequently, it melts at the high temperatures. Determination of the new stable phases that occur due to the change in the boron minerals by heating is important in the boron

technologies.

The kinetic mechanism of the thermal decomposition of the boron minerals has been the subject of numerous studies because of its fundamental interest and importance in the production of the boron compounds. The resulting anhydrous borate properties and its broad range of industrial uses depend strongly on the dehydroxylation conditions. Thus, the kinetic mechanism of dehydroxylation must be known.

Although one study about the decomposition kinetics of tunellite is found in the literature, to our knowledge so far there is no study related to the dehydroxylation kinetics of this mineral. Erdogan et al. analyzed some boron minerals (howlite, ulexite, and tunellite) using DTA/TG methods. The dehydration kinetics of tunellite was determined at a constant heating rate with the assumption of a first-order reaction [10].

The purpose of this study is to investigate the thermal stability and the mineralogical and structural changes of tunellite by means of heating. Specifically, in this study new stable phases were determined through heating and the conditions of production of those new stable phases were investigated. In addition, this study also focuses on the non-isothermal dehydroxylation kinetics of tunellite using 21 solid-state mechanisms.

*To whom all correspondence should be addressed.

Results and Discussion

DTA/TG Analyses

The TG/DTG curves of tunellite in N₂ atmosphere at 20°C/min heating rate are shown in Fig. 1. It was observed that the thermal decomposition of tunellite proceeded in a few separate stages:

- 1) Release of crystalline water, called dehydration, at 50 – 153°C
- 2) Release of the remaining crystalline water that is shown as two partly overlapping peaks on the DTG curve, which occurred at around 153 – 408°C
- 3) The slow release of the remaining OH groups from the polyanion structure, called dehydroxylation, up to 718°C.

XRD Analyses

The XRD patterns of the natural and calcined tunellite samples are illustrated in Fig. 2. The characteristic peaks of natural tunellite were observed at 6.51 Å, 3.85 Å, and 2.50 Å (PDF: 01-074-1638) from the XRD pattern (Fig. 2a). After calcination at 400°C, all the reflections due to the tunellite phase vanished and all the detected peaks were indexed to anorthic strontium boron hydroxide (PDF: 01-074-2286) and monoclinic strontium boron hydroxide (PDF: 01-074-2316). Thus, the dehydration process was completed at this temperature, as revealed by the DTA/TG analysis. As shown in Fig. 2c, the peaks of the powder were broad, thereby implying that the powder was

incompletely crystallized. The broad peaks were indexed to strontium borate (PDF: 01-074-2316) and veatchite (PDF: 01-074-2316). The peaks became sharp and narrow, as shown in Fig. 2d, which indicated that the powder crystallized better after calcination at 800°C. By increasing the calcination temperature from 710°C to 800°C, the intensities of the veatchite peaks increased. This indicated that it was necessary to heat the samples below the melting temperature to obtain only veatchite phase.

SEM Analyses

Fig.3 demonstrates the SEM images of the natural and calcined tunellite samples at 1000 magnification. In Fig. 3a, the structure of the natural sample presents the particles that are plate-like in shape and not uniform in size. Although, there was a decrease in the size of the structure and the irregular shapes of the particles were detected to be plate-like, the structure could still be observed after calcination at 400°C (Fig. 3b). As the calcination temperature was increased to 710°C, the structure transformed into a structure with a very spongy texture, containing open pores (Fig.3c). Comparison of the images revealed that when the sample was calcined at 800°C, the structure became more compact (Fig.3d). Thus, it was observed that an aggregation of the particles took place when the calcination temperature was increased. The obtained result was consistent with the BET surface area analysis, where an increase in the calcination temperature resulted in a decrease in the surface area.

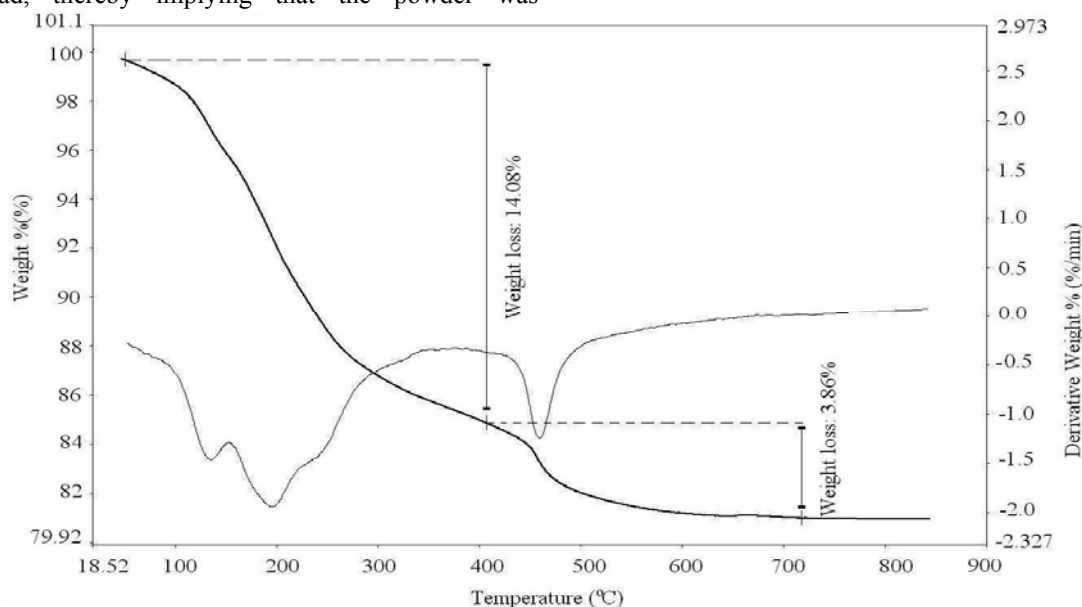


Fig. 1: TG/DTG curves for decomposition of tunellite at 20°C/min.

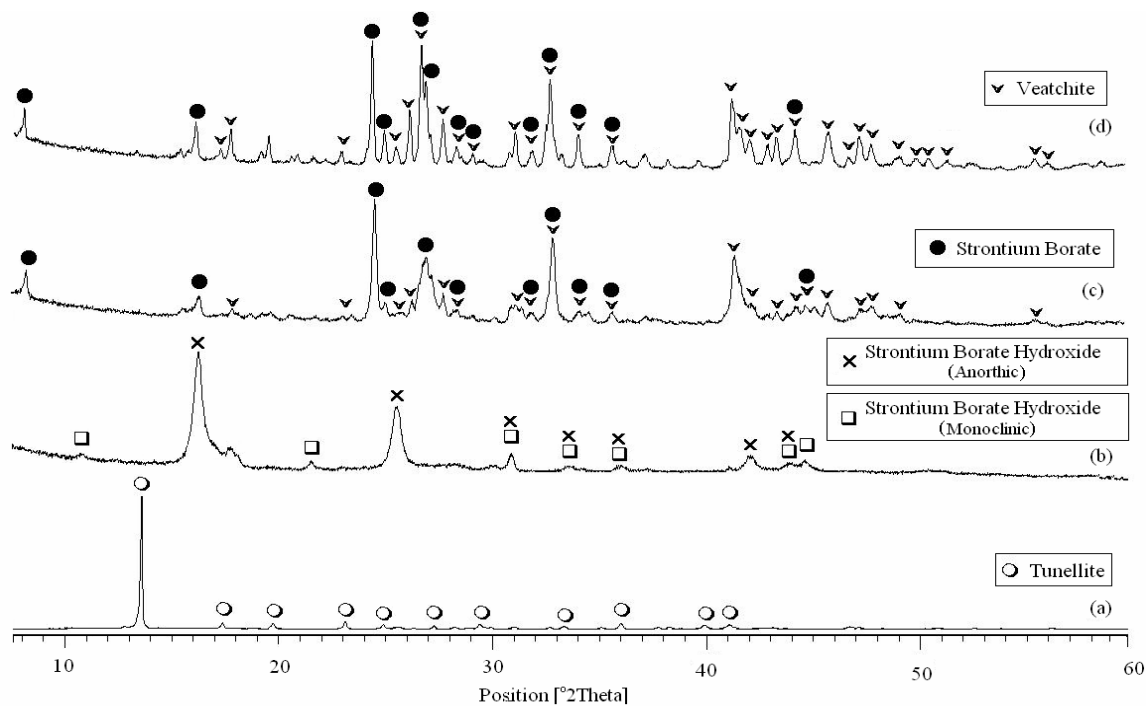


Fig. 2: Powder XRD patterns of heat treated tunellite samples: (a) natural, (b) Tun₄₀₀, (c) Tun₇₁₀, (d) Tun₈₀₀.

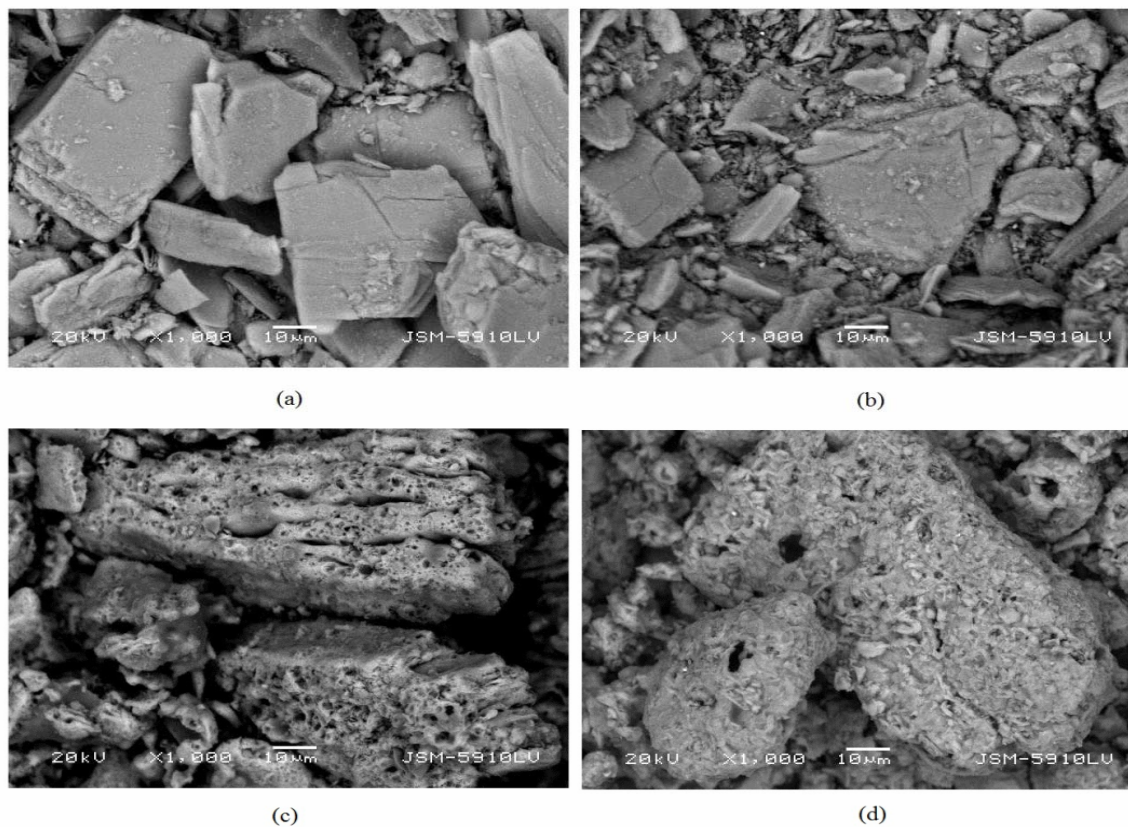


Fig. 3: SEM images of (a) natural tunellite, (b) Tun₄₀₀, (c) Tun₇₁₀, (d) Tun₈₀₀

BET Analyses

The specific surface area of the natural and calcined samples is plotted in Fig. 4, as a function of the calcination temperature. The BET-specific surface area increased from 2.41 m²/g to 2.62 m²/g due to thermal dehydration, thereby leading to smaller crystallites when the temperature was increased from 25°C to 400°C. By increasing the calcination temperature from 400°C to 800°C, the surface area decreased from 2.62 m²/g to 0.38 m²/g due to the shrinkage of the agglomerates.

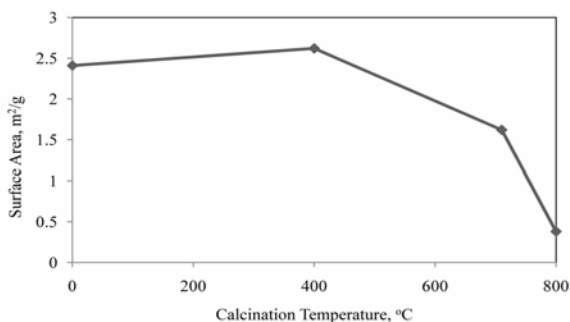


Fig. 4: Effect of calcination on the specific surface area of tunellite.

The Dehydroxylation Kinetics

The kinetic parameters of dehydroxylation of the tunellite, computed from the non-isothermal TG data, and based on the various mechanisms in integral forms are listed in Table-1. The obtained results indicated that the best correlation coefficients were observed in the third-order equation (F_3), with integral form $g(\alpha) = 1/(1 - \alpha)^2$, for all the heating rates.

The plot of $\ln A$ against E at three heating rates in the dehydroxylation stage of the tunellite is shown in Fig. 5. A high correlation exists between $\ln A$ and E , which proves the presence of KCE while the heating rates are varied, as shown in Fig. 5. The following expression is used to describe the KCE of the dehydroxylation stage:

$$\ln A = 0.1843E - 2.3161, R^2 = 0.9999 \quad (1)$$

Experimental*Sample Preparation and Characterization*

The investigated mineral was provided from the region of Kırka, Eskisehir, in Turkey. After manually cleaning the mineral of visible impurities, it was crushed, ground, and then sieved to give a particle size below 250 mesh by American Society

for Testing And Materials (ASTM) standard sieve. In order to investigate the effect of calcination on the structural properties of tunellite, the samples were calcined in a high temperature furnace at 400, 710, and 800°C for 5 h and named as Tun₄₀₀, Tun₇₁₀, and Tun₈₀₀, respectively. The calcination temperatures were determined according to the DTA/TG curves.

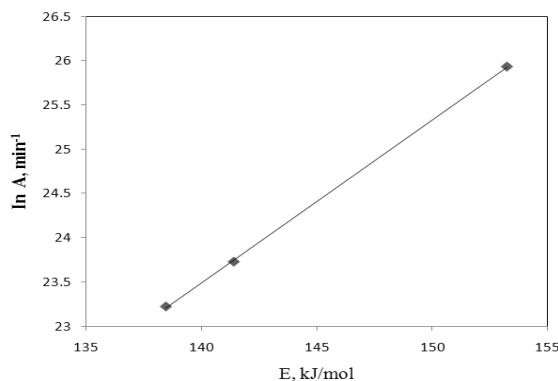


Fig. 5: KCE for dehydroxylation stage of tunellite

After the calcinations, the samples were cooled down to room temperature in a desiccator for the purpose of characterization analysis. When the tunellite was calcined at different temperatures, the color of the sample changed due to the effect of heating on the structure. First, the white color tunellite turned to gray after it was calcined to 400°C. Next, the color of the sample became bleached while increasing the temperature. Finally, it turned to a white color again at 800°C.

Thermogravimetric analyses were performed in the temperature range of 30 to 900°C, in a steam of nitrogen atmosphere, with a Perkin Elmer Diamond TG/DTA instrument. The above mentioned instrument was calibrated using the melting points of indium (156.6°C) and tin (231.9°C) as the standard substances under the same conditions as the sample. The conditions required for the experiment were as follows: a platinum crucible, nitrogen atmosphere with 150 ml/min flow rate, and heating rates of 10, 15, and 20°C/min.

The phase identification of the natural and calcined samples was determined by XRD analysis on a Philips PANalytical X'Pert Pro instrument with CuK α radiation. The X-ray diffractometer was operated at a generator voltage of 45 kV, a current of 40 mA, 2 θ values varying from 10° to 60°, with a step size 0.02°, and a speed of 1°/min. The International Center for Diffraction Data (ICDD and ICSD) base that was available in the X'Pert High Score Plus, was used for the purpose of quantification of the samples.

Table-1 Obtained kinetic parameters of dehydroxylation stage at different heating rates

No	10 °C/min			15 °C/min			20 °C/min		
	E (kJ/mol)	ln A (min ⁻¹)	R ²	E (kJ/mol)	ln A (min ⁻¹)	R ²	E (kJ/mol)	ln A (min ⁻¹)	R ²
1	3.42	-4.55	0.1891	2.11	-4.87	0.0655	3.84	-3.71	0.1517
2	8.71	-2.82	0.4661	7.06	-2.94	0.3115	9.37	-2.01	0.3883
3	19.31	-0.44	0.6608	16.97	-0.61	0.5424	20.42	0.41	0.5767
4	82.89	10.53	0.8042	76.45	9.59	0.7328	86.76	11.63	0.7361
5	114.68	15.61	0.8162	106.19	14.27	0.7492	119.92	16.85	0.7504
6	11.28	-1.97	0.7091	9.79	-2.00	0.5712	12.29	-1.09	0.6282
7	19.20	-0.18	0.8023	17.31	-0.26	0.7046	20.64	0.73	0.7311
8	35.04	2.93	0.8598	32.343	2.70	0.7904	37.33	3.92	0.8004
9	153.54	20.56	0.8828	144.08	18.98	0.8314	161.63	22.15	0.8310
10	70.53	7.94	0.8628	65.66	7.29	0.8023	74.44	9.09	0.8055
11	65.12	7.32	0.8434	60.36	6.69	0.7777	68.62	8.41	0.7820
12	128.04	19.67	0.9616	122.33	18.76	0.9344	136.58	21.40	0.9342
13	51.10	5.29	0.7771	46.71	4.75	0.6959	53.59	6.26	0.7043
14	12.80	-1.13	0.9438	11.84	-1.02	0.9154	14.35	-0.15	0.9344
15	6.45	-2.95	0.8997	5.70	-2.84	0.8491	7.57	-1.97	0.9015
16	131.50	18.03	0.8477	122.50	16.58	0.7876	137.91	19.42	0.7880
17	16.94	0.74	0.8465	15.34	0.72	0.7575	18.38	1.66	0.7849
18	138.73	17.86	0.8605	129.57	16.36	0.8035	145.69	19.30	0.8036
19	82.55	11.31	0.8969	77.45	10.59	0.8463	87.40	12.57	0.8480
20	64.47	9.48	0.9861	62.86	9.39	0.9920	70.25	10.95	0.9930
21	141.41	23.73	0.9883	138.48	23.22	0.9935	153.24	25.93	0.9942

The SEM observations were carried out on a JEOL (JSM 5410 LV) to determine the morphological characteristics of the calcined samples.

The Brunauer–Emmett–Teller (BET) surface areas of the natural and calcined minerals were evaluated by a multipoint BET method using the adsorption data in a Kelvin 1042 Sorptometer (Costech Microanalytical).

Kinetic Analysis Theory

The dehydration and dehydroxylation of minerals are a solid state process of the type:
A (solid) → B (solid) + C (gas)

The most commonly used expression to describe the reaction rate in the solid-state transformations is:

$$\frac{d\alpha}{dt} = \beta \cdot \frac{d\alpha}{dT} = k(T) \cdot f(\alpha) \quad (2)$$

where β is the heating rates (°C/min), $f(\alpha)$ and $k(T)$ are functions of conversion and temperature, respectively. The temperature dependence of the rate constant, $k(T)$, is described by the Arrhenius equation:

$$k(T) = A \cdot e^{\left(-\frac{E}{RT}\right)} \quad (3)$$

where E is the activation energy (kJ/mol), A is the pre-exponential factor (min⁻¹), and R is the gas

constant (8.314 J/K.mol). Replacing Eq. 2 into Eq. 1 gives:

$$\frac{d\alpha}{dT} = \frac{A}{\beta} e^{\left(-\frac{E}{RT}\right)} f(\alpha) \quad (4)$$

By integration of this equation the following expression was obtained:

$$g(\alpha) = \int_0^{\alpha} \frac{d\alpha}{f(\alpha)} = \frac{A}{\beta} \int_{T_0}^T e^{\left(-\frac{E}{RT}\right)} d(T) \quad (5)$$

where T_0 is the initial temperature corresponding to conversion rate α_0 and T is the peak temperature corresponding to conversion rate α . Several techniques have been used for the evaluation of the right-hand side integral. Most commonly used method for this purpose is integral method of Coats and Redfern. This method has been successfully used for studies on the kinetic analysis of different solid materials. The kinetic analysis parameters can be calculated by employing the Coats and Redfern relation [11].

$$\ln \left[\frac{g(\alpha)}{T^2} \right] = \ln \left[\frac{AR}{\beta E} \right] - \frac{E}{RT} \quad (6)$$

where $g(\alpha)$ is a function, different expressions of a mechanism for various solid-state reactions (Table-2), α is the conversion rate of the reaction, that is,

$$\alpha = \frac{w_0 - w_t}{w_0 - w_{\infty}} \quad (7)$$

where w_0 , w_t , and w_∞ are the initial weight of the sample (mg), the sample weight at any temperature T , and the final sample weight (mg), respectively. When the correct $g(\alpha)$ is used, the plot $\ln[g(\alpha)/T^2]$ versus $1/T$ gives a straight line with the maximum correlation coefficient (R^2). Arrhenius parameters (E and A) can be computed from the slope and intercept of the linear plot [12-16]. Advantages of this method are that the order of the reaction is not assumed and all kinetic parameters are determined from experimental results.

Table-2: Reaction mechanisms to represent the solid state process.

	Reaction Model	$g(\alpha)$
1	Power law (P_1)	$\alpha^{1/4}$
2	Power law (P_2)	$\alpha^{1/3}$
3	Power law (P_3)	$\alpha^{1/2}$
4	Power law (P_4)	$\alpha^{3/2}$
5	One-dimensional diffusion	α^2
6	Avrami-Erofeev equation (A_2)	$[-\ln(1-\alpha)]^{1/4}$
7	Avrami-Erofeev equation (A_3)	$[-\ln(1-\alpha)]^{1/3}$
8	Avrami-Erofeev equation (A_4)	$[-\ln(1-\alpha)]^{1/2}$
9	Three-dimensional diffusion	$[1-(1-\alpha)^{1/3}]^2$
10	Contracting sphere	$1-(1-\alpha)^{1/3}$
11	Contracting cylinder	$1-(1-\alpha)^{1/2}$
12	Second-order	$(1-\alpha)^{-1}-1$
13	Contracting linear	α
14	Contracting area	$[1-\ln(1-\alpha)]^{1/2}$
15	Contracting volume	$[1-\ln(1-\alpha)]^{1/3}$
16	Two-dimensional diffusion (D_2)	$(1-\alpha)\ln(1-\alpha) + \alpha$
17	Three-dimensional diffusion (D_3)	$[1-\ln(1-\alpha)]^{1/3}$
18	Bronstein-Ginstling diffusion (D_4)	$(1-2\alpha/3) - (1-\alpha)^{2/3}$
19	First-order reaction (F_1)	$-\ln(1-\alpha)$
20	Second-order reaction (F_2)	$1/(1-\alpha)$
21	Third-order reaction (F_3)	$1/(1-\alpha)^2$

The KCE is evaluated for the dehydroxylation stage at different heating rates for correlating the kinetic parameters. KCE can be described in the following expression,

$$\ln A = aE + b \quad (8)$$

where a and b are constants

Conclusion

In the present study, the mineralogical and structural changes in the structure of tunellite under heating were investigated and the kinetic mechanism of the dehydroxylation process was examined by using different equations. In conclusion, the following points need to be highlighted from this study:

- It was found that the thermal decomposition of tunellite occurred in three dehydration and one dehydroxylation stages between 51 and 718°C.
- When the natural tunellite was heated to 400°C, the tunellite phase was completely transformed into anorthic and monoclinic strontium borate hydrate.
- By the increase of calcination temperature from 400 to 710°C, new stable phases (veatchite and strontium borate) were observed. With further increase in the calcination temperature from 710 to 800°C, the veatchite content also increased. Thus, the best way to obtain veatchite in a single phase was to increase the calcination temperature to below melting point.
- XRD and SEM analyses results showed that the mineral structure became more compact with the increase of the veatchite content.
- Variation in calcination temperatures had an important effect on the properties of tunellite. By increasing the calcination temperature, more aggregated particles were found in the sample than when it was calcined at a low temperature, as observed by the microstructural changes of tunellite using SEM analysis.
- The SEM analysis results were in accordance with the BET surface area analysis. It was observed that the calcination temperatures had an obvious influence on the BET surface areas of the samples.
- The most probable model function of the dehydroxylation stage was found to be the third-order reaction (F_3), which gave an appropriate kinetic description for the dehydroxylation stage. The average activation energy for tunellite was computed as 144.38 kJ/mol through the non-isothermal dehydroxylation studies.
- A linear relationship was observed between the obtained activation energies and the pre-exponential factors at different heating rates, which proved the presence of KCE.
- The investigation of new stable phases, the thermal behavior and dehydroxylation kinetics of tunellite give an idea about the usage of this mineral in the production of boron compounds. It is hoped that this study will be helpful in the usage of tunellite in industrial applications.

References

1. C. Helvacı, R. N. Alonso, *Turkish Journal of Earth Sciences*, **9**, 1 (2000).
2. O. Baysal, *Bulletin of the Mineral Research and Exploration Institute of Turkey*, **79**, 22 (1972).
3. J. R. Clark, *American Mineralogist*, **49**, 1549 (1964).
4. D. J. Doon, L. D. Lower, Kirk Othmer Encyclopedia of Chemical Technology, Interscience, New York, (1971).
5. S. Piskin, Ph.D. Thesis, Thermal Properties of Hydrated Boron Minerals, University of Istanbul Technical (1983).
6. G. Ataman, O. Baysal, *Congress of earth sciences on the occasion of the 50. Anniversary of Turkish Republic MTA Institute*, Ankara, 537 (1973).
7. S. Şener, G. Ozbayoglu, and S. Demirci, *Thermohimica Acta*, **362**, 107 (2000).
8. O. Yildiz, *Powder Technology*, **142**, 7 (2004).
9. H. Gulensoy and T. Teberdar, *Bulletin of the Mineral Research and Exploration Institute of Turkey*, **79**, 30 (1972).
10. Y. Erdogan, A. Zeybek, A. Sahin, and A. Demirbas, *Thermohimica Acta*, **326**, 99 (1999).
11. W. Coats and J. P. Redfern, *Nature*, **201**, 68 (1964).
12. S. Vyazovkin, C. A. Wight, *Thermohimica Acta*, **53**, 340 (1999).
13. Y. Tonbul, A. Saydut, K. Yurdakoc, and C. Hamamcı, *Journal of Thermal Analysis and Calorimetry*, **95**, 197 (2009).
14. E. Kaya, *Journal of The Chemical Society of Pakistan*, **33**, 555 (2011).
15. G. Hussain and M. A. Khan, *Journal of The Chemical Society of Pakistan*, **33**, 317 (2011).
16. D. H. He, J. T. Chen, Y. Y. Di, Z. P. Chen, D. Q. Wang and W. Y. Dan, *Journal of The Chemical Society of Pakistan*, **33**, 333 (2011).